Materials Chemistry and Physics 324 (2024) 129696

Contents lists available at ScienceDirect

Materials Chemistry and Physics

journal homepage: www.elsevier.com/locate/matchemphys

Fabrication and characterization of Zinc-xTitanium alloys by SPS for biodegradable implants: A comparative study on corrosion resistance and biological behavior

Seyed Amirhossein Salahi [a], Nahid Hassanzadeh Nemati [a,*], Sayed Khatiboleslam Sadrnezhaad [b], Ghasem Najafpour Darzi [c]

[a] Department of Biomedical Engineering, Science and Research Branch, Islamic Azad University, Tehran, Iran
[b] Department of Materials Science and Engineering, Sharif University of Technology, Tehran, Iran
[c] Department of Chemical Engineering, Babol Noshirvani University of Technology, Babol, Iran

HIGHLIGHTS

- This study explored the fabrication and characterization of two novel zinc-titanium-based alloys (4 and 10 wt% Ti) that underwent mechanical alloying and were shaped using the spark plasma sintering (SPS) method.
- Corrosion tests demonstrated superior corrosion resistance in the Zn–4Ti alloy compared to the Zn–10Ti alloy.
- Cell toxicity tests, conducted indirectly through extraction processes, indicated lower toxicity in the Zn–4Ti alloy.
- The alloy containing 4 wt% titanium shows promise as a viable candidate for producing biodegradable implants.

ARTICLE INFO

Keywords:
Zinc-titanium
Mechanical alloying
Spark plasma sintering
Biodegradable implants

ABSTRACT

This study investigated the fabrication and characterization of two new zinc-titanium-based alloys. The Zn-xTi alloys (x = 4 and 10 wt%) were mechanically alloyed by powder metallurgy for 10 h. The spark plasma sintering (SPS) method shaped the resulting powder. The fabricated samples were evaluated in terms of morphology and structure by XRD, SEM, and microhardness tests. The obtained parts' corrosion resistance and biological behavior were also examined by potentiodynamic polarization analysis, electrochemical impedance spectroscopy (EIS), and MTT tests. The results showed that alloying increased the hardness compared to pure zinc samples. The corrosion test results indicated higher corrosion resistance of Zn–4Ti alloy than Zn–10Ti alloy. The cell toxicity test, performed indirectly by the extraction process, clearly showed lower toxicity of Zn–4Ti alloy compared to the other alloy. In the extractions with low concentrations (25 % and 12.5 %), no cell toxicity was observed in the Zn–4Ti alloy. This research concludes that the alloy containing 4 wt% titanium can be a suitable candidate for making biodegradable implants.

1. Introduction

Bone is one of the few tissues that can regenerate after damage. Regeneration is done by a series of complex physiological processes that lead to a balance between osteoblast and osteoclast cells [1,2]. With the increase in the elderly population and aging, millions of people are affected by bone diseases and traumas caused by accidents. Researchers seek the best materials and methods to replace and treat bone defects [3,4]. Bone grafts are the second most common tissue transplants after blood. This method leads to bone tissue formation, reconstruction, and repair in case of defects and fractures. However, these grafts have disadvantages, such as using bone, harvesting sites, and transmitting diseases and other infectious factors from the donor [2,5]. Using biomaterials in bone scaffold applications has advantages such as biocompatibility, bioactivity, osteoconductivity, and osteoinduction. It is an attractive method for replacing, repairing, and treating bone and dental defects [5],[7]. These materials can be extracted from natural materials [8] or synthesized by mimicking hierarchical structures of

* Corresponding author.
E-mail addresses: Nahid_Hasanzadeh@yahoo.com, hasanzadeh@srbiau.ac.ir (N. Hassanzadeh Nemati).

https://doi.org/10.1016/j.matchemphys.2024.129696
Received 17 February 2024; Received in revised form 6 July 2024; Accepted 8 July 2024
Available online 9 July 2024

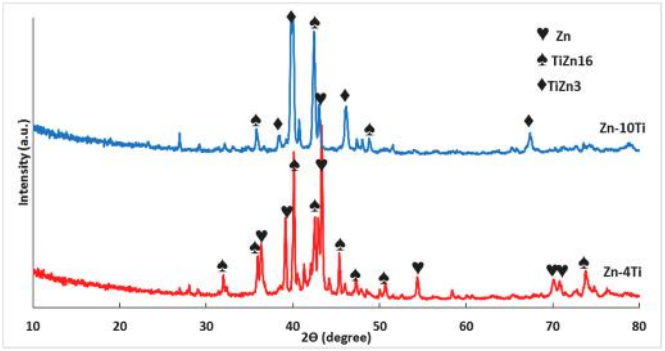

Fig. 1. XRD results of Zn–10Ti and Zn–4Ti alloys.

synthetic materials [9]. Due to the replacement with bone tissue, the strength and modulus of biomaterials should be acceptable.

Traditional bone substitute materials such as bioactive glasses and natural and synthetic polymers have disadvantages such as insufficient strength, high absorption rate, and undesirable reactions with tissue [10]. Stainless steel, cobalt-chrome alloy, and titanium alloys are three high-strength biometals among the joint implants used. However, these metals require second surgery to be removed from the body due to their non-absorbability and stress shielding phenomenon. Therefore, using alternative metals without the mentioned problems has been considered [11,12]. Some surface modifications have improved their biological behaviors [13,14], but their non-biodegradability has still challenged their use in short-term applications. Three biodegradable metals, magnesium, zinc, and iron, with different biological roles and degradation rates, have overcome the mentioned problems. They support the healing process by gradually degrading from the environment after complete tissue recovery.

Pure zinc has a suitable degradation rate for biodegradable implants, but its mechanical properties are inadequate compared to bone tissue, limiting its clinical applications [15,16]. Recent research has focused on alloying zinc with other elements to improve its mechanical properties and use it in scaffold engineering for bone tissue [17]. Some of the alloying elements used in zinc metal are copper [18], zirconium [19], lithium [20], silver [21], aluminum [22], magnesium [23], iron [24], magnesium and calcium [25], magnesium and strontium [26], magnesium and silver [27], copper and iron [28]. Titanium is one of the elements added to zinc to increase its mechanical strength. When Zinc is alloyed with Titanium, it boosts osteogenic activity by releasing of Zn^{2+} ions [29]. Creating a Zinc–Titanium alloy has achieved good results in terms of strength criteria for implants in osteosynthesis [30]. Zinc also holds promise in addressing the significant issue of in-stent restenosis, a condition that can lead to the failure of stent implants [31]. As a result, these alloys hold great potential as biodegradable materials for use in vascular stents. Yin et al. showed that the eutectic phase of zinc with intermetallics was formed at the boundaries of primary grains. The hardness and strength of this alloy increased with increasing titanium due to the formation of the TiZn16 intermetallic phase [32]. Wang et al. showed that by increasing the amount of titanium, the hardness and corrosion rate of the alloy increased through two methods of casting and casting along with hot rolling [33]. The casting process has disadvantages, such as creating unwanted chemical reactions between the elements present in the alloy. Powder metallurgy has overcome this limitation by performing the process at temperatures lower than the melting point of the elements and the ability to produce different compositions with lower costs [34]. Extensive research has been done in the field of zinc alloying by powder metallurgy, including compositing zinc with magnesium oxide [35], calcium silicate [36], copper-calcium [37], copper-titanium [38], and graphene [39]. For preparation of Zinc and Zinc alloys, some methods have used including selective laser melting (SLM), and spark plasma sintering (SPS). SPS offers distinct advantages over other methods due to its ability to operate at lower sintering temperatures, achieve higher heating rates, shorten sintering durations. These benefits collectively contribute to enhancing the physical, mechanical, chemical, thermal and tribological properties in materials fabricated through this technique [40,41]. For optimal bone integration and cell infiltration, biomaterials could be engineered with a porous structure. Porous zinc scaffolds exhibit strong antibacterial properties, making them effective at combating and eliminating

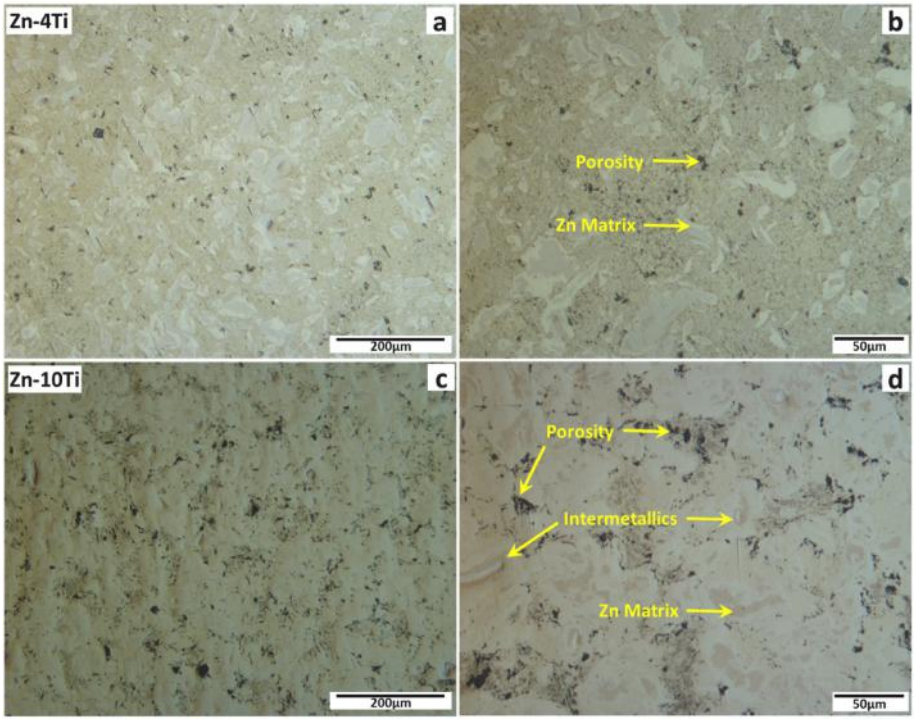

Fig. 2. Optical microscope images: Zn–4Ti (a,b) and Zn–10Ti (c,d) samples in different magnifications.

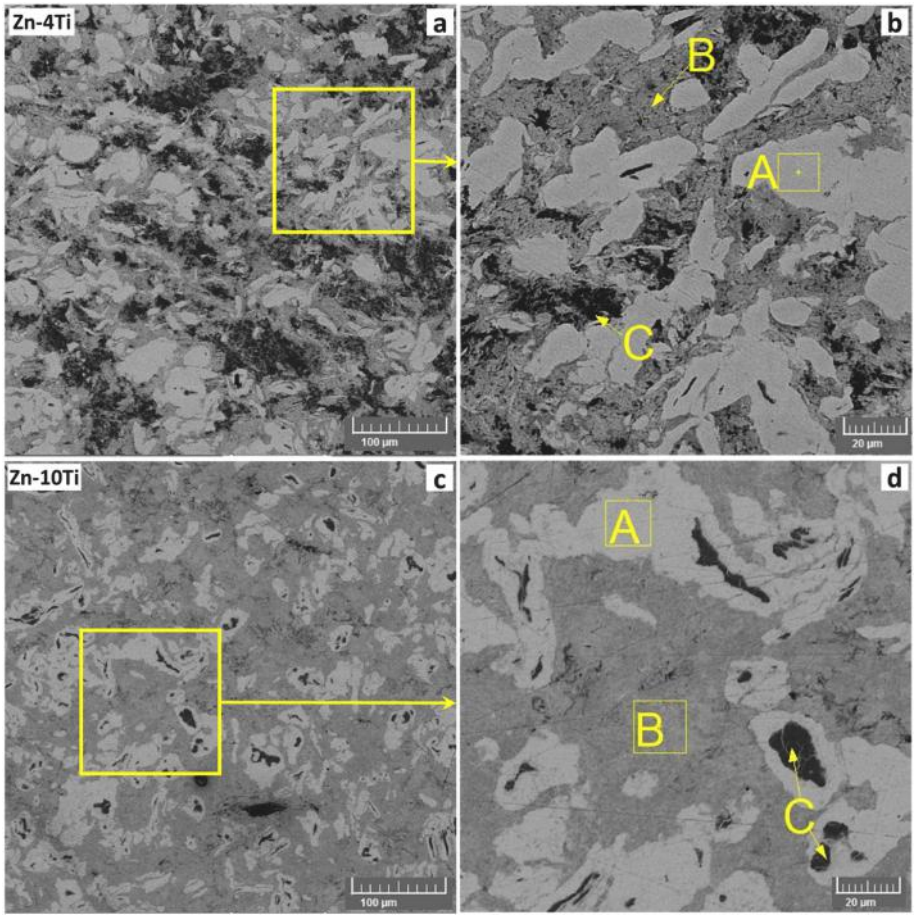

Fig. 3. SEM images of Zn–4Ti (a,b) and Zn–10Ti (c,d) samples.

Table 1
EDS results of Zn–10Ti and Zn–4Ti samples.

Sample Element (at %)	Zn–4Ti			Zn–10Ti		
	A	B	C	A	B	C
Ti	8.64	16.92	42.55	12.31	26.07	95.31
Zn	91.36	83.08	57.45	87.69	73.93	4.69
Zn/Ti	10.57	4.91	1.35	7.12	2.84	0.05
The closest intermetallic compounds	TiZn16 TiZn10	TiZn3 TiZn5	Ti2Zn3 TiZn	Ti3Zn22 TiZn7	TiZn2 TiZn3	Ti2Zn Ti(α)

bacterial infections [29]. So, SPS processing can help produce a porous structure. However, research has yet to be done on the mechanical alloying of zinc-titanium compound and the fabrication of parts obtained from it by the spark plasma sintering (SPS) method, which is addressed in this study. The resulting samples were investigated in terms of morphological, structural, corrosion, mechanical, and biological behavior. The aim of developing these alloys is to use them in making biodegradable implants.

2. Experimental procedure

2.1. Material preparation

To make Zn–Ti alloy by mechanical alloying, pure zinc powder (<45 μm) and pure titanium powder (<150 μm) (Merck, Germany >98 %) were used. The powders were measured with ratios of 10 and 4 wt% titanium (known as Zn–10Ti and Zn–4Ti, respectively) and poured into separate cups. Then, the alloying process was performed by a planetary mill machine (Amin Asia Fanavar Pars model NARYA-MPM-250H, Iran) for 10 h under an argon atmosphere with a ball-to-powder weight ratio of 10:1. The rotation speed of the device was 400 rpm, and for every 10 min of working, 5 min of rest was given. 2 % stearic acid by weight was added as a control agent to prevent excessive cold welding. After finishing the milling process, the powders were heated by an SPS device (Hijoy, China) under argon gas with a pressure of 45 MPa and speed of 10° per minute up to 340 °C and then sintered for 10 min at this temperature. After sintering, cylindrical samples obtained with a diameter of 10 and thickness of 2 mm were cooled for 30 min in a furnace up to room temperature. Then, the samples were sanded up to number 2000 and polished using diamond paste/alumina nanoparticles. Finally, they were ultrasonicated in ethanol and acetone to clean and degrease the samples and dried in air. Chemical etching was done with 0.5 % HNO_3 solution for 15 s. The microstructure of the samples was investigated by an SEM device (LEO VP 1450 model made by Germany) equipped with an EDS detector. XRD analysis (PW3710 Philips, Netherlands) with Kα from monochromatic copper with scan speed 0.5/sec and scan step 0.02° was performed to identify the phases. Vickers microhardness testing (Poyesh Sanat Company, Iran) was performed by applying a force of 2 kg with a dwell time of 15 s. The reported result is the average of three measurements. Electrochemical corrosion of the samples was evaluated by polarization test using PG STAT 302 N device in simulated body fluid (SBF) solution with a scan rate of 0.1 mV per second (against calomel reference electrode). In order to evaluated the cytotoxicity of samples, the specimens were sterilized by autoclave. The ISO10993-12 protocol was followed for the extraction procedure. Samples were exposed to culture media at 37 °C for 7 days, with 1 ml of culture media added for every 3 cm^2 of the sample's surface. The biological evaluation

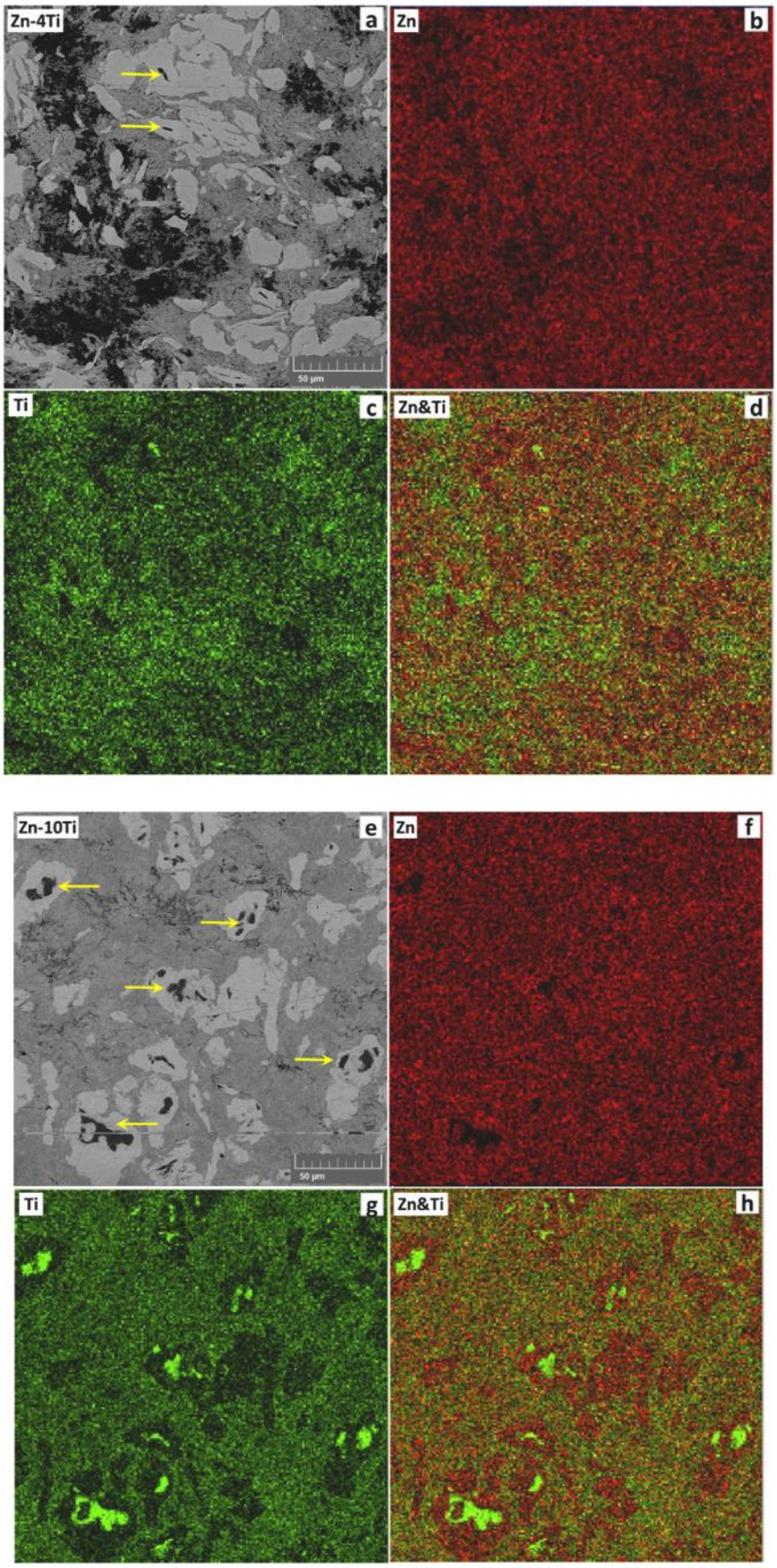

Fig. 4. EDS elemental map results of Zn–4Ti (a–d) and Zn–10Ti (e–h) samples.

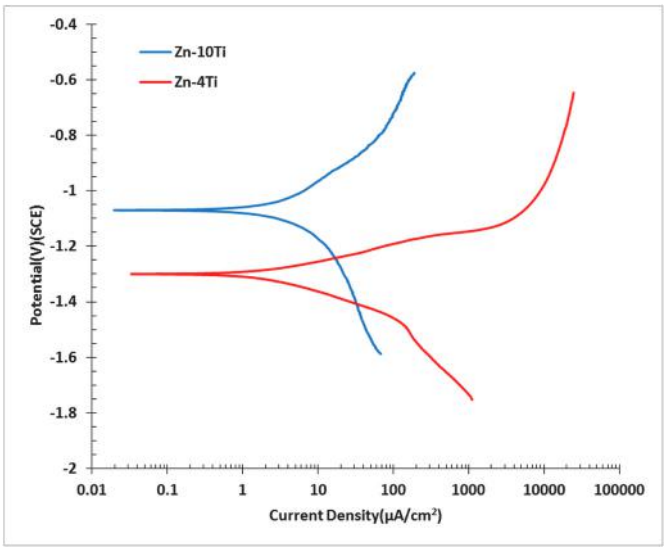

Fig. 5. Polarization diagram of Zn–10Ti and Zn–4Ti samples.

Table 2
Polarization test data for Zn–10Ti and Zn–4Ti samples.

Samples	βa (mV)	βc (mV)	I_o (μA/cm^2)	E_o (V)	V_{Corr} (μm/y)
Zn–4Ti	61.36	−86.69	1.8227	−1.3003	27
Zn–10Ti	164.85	−172	2.2989	−1.0705	35

was conducted using the human osteoblast cell line MG-63 (NCBI; National Cell Bank of Iran). MG-63 cells were cultured in DMEM (Gibco, USA) with 100 U. ml^{-1} penicillin, 10 % (v/v) fetal bovine serum (FBS, Gibco, USA), and 100 g ml^{-1} streptomycin, in a 37 °C, humidified atmosphere with 5 % CO2. Initially, cells were seeded into a 96-well plate (SPL, Korea) with 100 μl of culture media containing 104 MG-63 cells per well. After 24 h, the culture medium was replaced with various dilutions of the sample (100 %, 50 %, 25 %, and 12.5 %). Following another 24 h, the solution was substituted with 100 μL of 0.5 mg. ml^{-1} MTT solution and kept in an incubator for 4 h. Subsequently, the solution was aspirated, and 100 μL of isopropanol (Sigma, US) was added to the wells, which were then placed in a shaker incubator for 15 min. In conclusion, the multiwell plate was positioned in an ELISA reader (BioTek ELx808, USA), and the absorbance at a wavelength of 570 nm was measured. Cell viability was assessed by normalizing the results relative to the negative control (DMEM).

3. Results and discussion

Fig. 1 shows the XRD results of Zn–10Ti and Zn–4Ti alloys.

No metal ion contamination, such as iron, cobalt, and chromium from stainless steel balls and cups in the mechanical alloying process, has diffused into the alloy structure while making Zn–10Ti and Zn–4Ti alloys. It should be noted that before the alloying process, pure zinc powder was milled for 5 h in the device chamber to form a thin layer of zinc metal on the surface of the device's cups and balls. With alloying, some of the peaks of pure zinc metal (35.758, 39.717, 43.410, 54.286, 70.007, 70.550) have been reduced, and many peaks have not appeared, and their intensity has also decreased.

In Zn–4Ti alloy, peaks of pure zinc and intermetallic phase TiZn16 were observed. The formation process of this phase is influenced by percentage of added titanium [42]. In the Zn–10Ti sample, by increasing the titanium percentage to 10 %, in addition to the prominent peaks of the intermetallic compound TiZn16, peaks of TiZn3 also appeared. In Zn–10Ti, the intensity of Zinc peaks also decreased. By increasing low amounts of titanium to zinc, the intensity of all the diffraction zinc matrix does not change and shows similar intensities with pure zinc [43]. However, if titanium is added to zinc in higher amounts, as can be

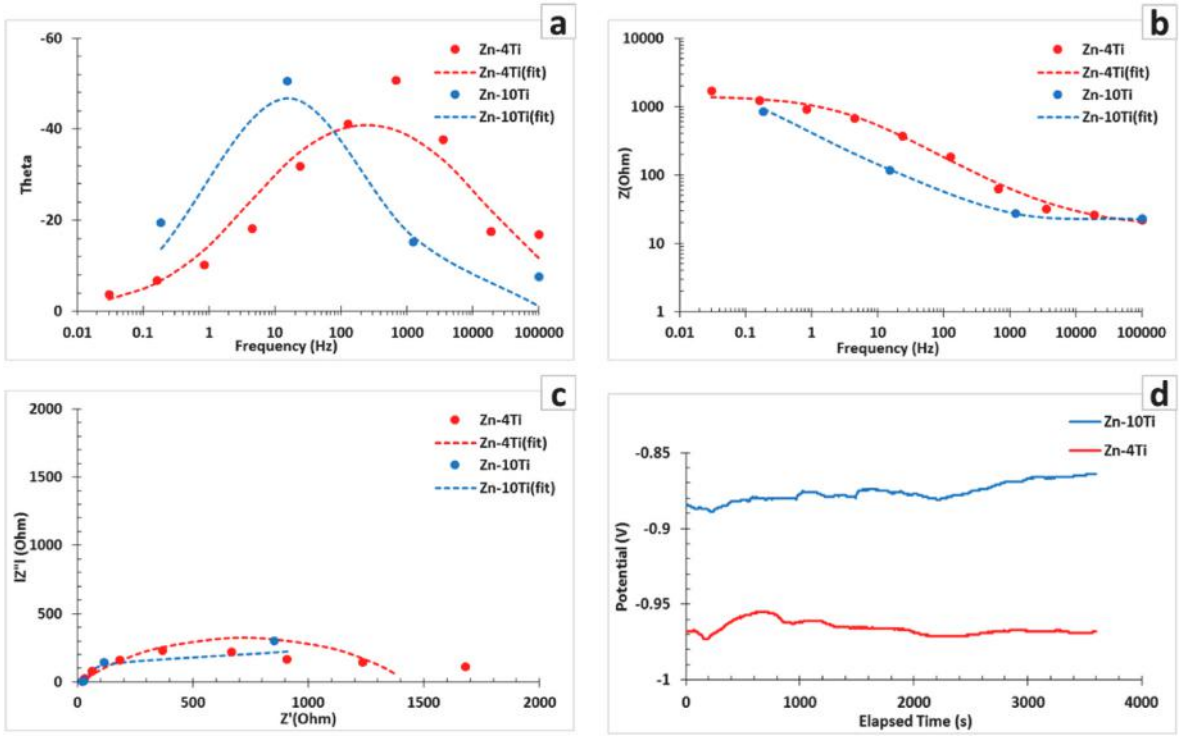

Fig. 6. Electrical impedance test results and open circuit potential of Zn–10Ti and Zn–4Ti samples; (a) Bode phase angle, (b) Bode module, (c) Nyquist and (d) OCP plots.

Table 3
Impedance test data and equivalent circuit.

	Rs	CPE-T	CPE-P	Rp
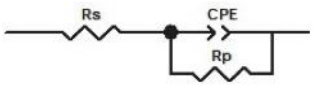				
Zn–4Ti	16.71	0.000114	0.55146	1411
Zn–10Ti	22.55	0.000275	0.66558	1102

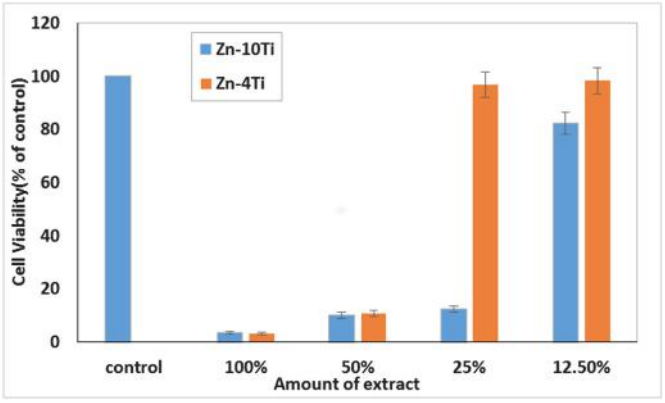

Fig. 7. Survival of MG-63 cell by indirect method in different extraction percentages for two alloy structures after 7 days in the culture media.

seen, the intensity of the zinc peaks decreases. According to the zinc-titanium phase diagram [44], two intermetallic compounds of TiZn5 and TiZn10 besides the intermetallic compounds obtained in Fig. 1 are possible to be present, but according to Mr. Okamoto's report [45], the crystal structure of these compounds are unknown Therefore, it was not identified, and other peaks in the XRD figure show the possibility of these two compounds. To prove this point, we have predicted the possibility of the presence of these intermetallic compounds by performing the EDS test that is discussed later.

Fig. 2 shows optical metallographic images of samples. Applying severe loads during milling and 45 MPa during the plasma arc processing deformed the initial spherical shape of the powders. Due to high pressure and temperature, diffusion opportunity at particle boundaries was provided, and an alloy structure was formed. Based on XRD results in Fig. 1, the formation of this alloy is confirmed.

Based on the Zn–Ti phase diagram, zinc has almost no solubility for titanium at room temperature, and multiple intermetallic compounds form even by adding a meager percentage of titanium to zinc [33,46]. The defects present in samples indicate the existence of pores that have yet to be eliminated during the press and sintering process [47]. As the size of Zn and Ti powders are <45 μm and <150 μm respectively, the size and distribution of remaining pores indicated by black color are more in Zn–10Ti alloy than Zn–4Ti alloy, related to the presence of more Ti powders in Zn–10Ti alloy [48]. Based on calculation by ImageJ software, the porosity percentage of Zn–4Ti alloy (1.85 %) is less than half the porosity percentage of Zn–10Ti alloy (4 %). Since in Zn–10Ti alloy, there is a higher percentage of titanium metal, and the initial size of this metal was higher than zinc metal size, we see more number, uneven distribution, and larger pore size compared to Zn–4Ti alloy. The thermal mismatch of two metals present in these alloys has also affected the formation of some of these pores [49].

Fig. 3 shows the SEM images of the two fabricated samples, Zn–10Ti and Zn–4Ti. Table 1 shows the EDS results of the phases identified in Fig. 3.

The SEM images of both alloys reveal the presence of intermetallic phases in these samples. In the images related to the Zn–10Ti alloy sample, the light-colored area indicates the presence of zinc metal and intermetallic compounds rich in zinc (less than 12 atomic percent of titanium). The black-colored area indicates intermetallic compounds rich in titanium metal (more than 50 atomic percent of titanium), and the gray-colored areas that are formed inside the light-colored areas indicate the presence of intermetallic phases between 12 and 50 atomic percent of titanium. In the Zn–4Ti alloy sample, the light-colored area with less than 12 atomic percent of titanium also indicates the presence of zinc metal and intermetallic compounds rich in zinc. The black-colored area indicates intermetallic compounds rich in titanium metal (less than 50 atomic percent of titanium), and the gray-colored areas indicate intermetallic phases in the range between 15 and 25 atomic percent of titanium. The planetary milling process formed these intermetallic compounds due to cold welding between the atoms of metal particles that diffuse each other under high mechanical impacts. Table 1 shows the closest intermetallic compounds based on the atomic percentage ratio of zinc to titanium.

Comparing the EDS analysis of two samples, it is observed that the black area in the Zn–10Ti sample contains more titanium than the Zn–4Ti structure and is consistent with previous works [50]. Fig. 4 shows the EDS elemental map of Zn–10Ti and Zn–4Ti samples. As can be seen, the titanium element is uniformly distributed in the matrix of the Zn–4Ti sample. Titanium has a higher percentage in areas marked with arrows than in adjacent areas. It is observed that the areas rich in titanium in the Zn–10Ti sample are much more than the Zn–4Ti sample. In the Zn–10Ti sample, in the vicinity of areas rich in titanium, there are areas rich in zinc, which indicates incomplete diffusion of these two elements under the process conditions. In total, titanium in the Zn–4Ti sample shows a more uniform distribution than Zn–10Ti alloy.

Vickers hardness test results for pure zinc metal have been reported 65 [51]. For Zn–10Ti and Zn–4Ti samples, hardness numbers were 237 and 125 Vickers, respectively, which have a high hardness compared to pure zinc. In Zn-0.3Ti alloy made by casting method [33], a hardness number of 59 Vickers was reported, which significantly differs from the hardness obtained in this research. The formation of multiple intermetallic compounds in these alloys, has probably led to a high hardness increase in this alloy structure due to adding titanium element to zinc metal. The intermetallic phase that titanium forms with zinc leads to the improvement of strength of the zinc-based alloy, but in high volume fractions, it can lead to the reduction of elongation in the alloy [52].

Fig. 5 shows the polarization test results of Zn–10Ti and Zn–4Ti samples. Corrosion potential E_{corr} and corrosion current density I_{corr} are given in Table 2.

The polarization test results show that the corrosion potential of Zn–10Ti and Zn–4Ti samples are equal to −1.0705 and −1.3003 V. The corrosion potential of the Zn–4Ti sample compared to pure zinc metal (−0.988 (50) has more negative corrosion potential. Corrosion current density values of Zn–10Ti and Zn–4Ti samples are respectively equal to 2.2989 and 1.8227 μA/cm^2, which have higher corrosion resistance than most binary alloys [33]. Electrical impedance test results and open circuit potential are shown in Fig. 6. Impedance test data and equivalent circuits are given in Table 3.

It is observed that the corrosion resistance of Zn–4Ti is slightly higher than Zn–10Ti. The formation of multiple intermetallic compounds in these alloys, affects corrosion resistance due to adding titanium element to zinc metal and creating a galvanic corrosion reaction.

Fig. 7 shows the cell toxicity results on different extracts from both

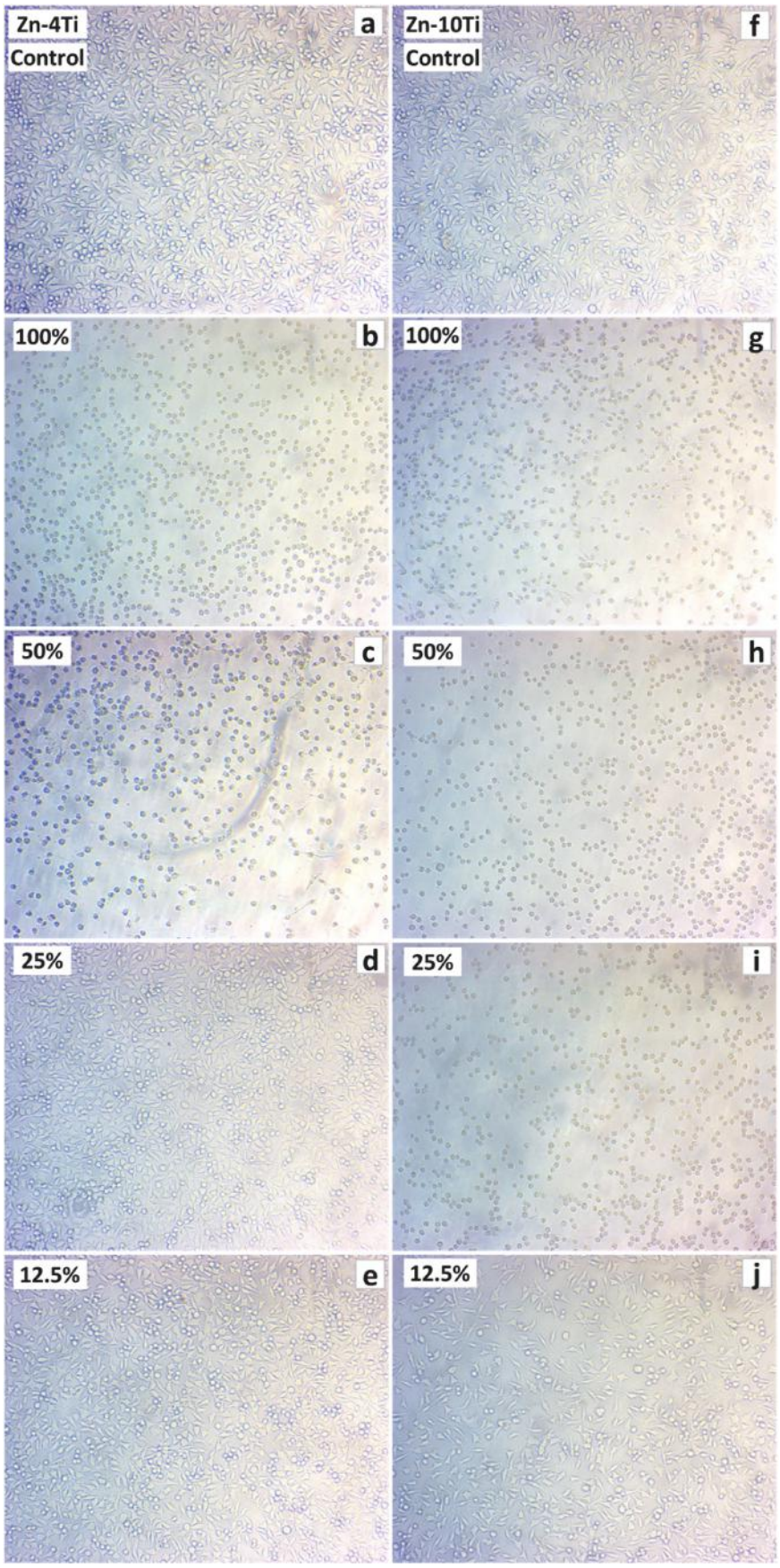

Fig. 8. Images of MG-63 cells after 7 days in the culture media of both alloys: (a,f) Control samples, (b,g)100 % (c,h) 50 % (d,i) 25 % and (e,j) 12.5 %.

Zn–10Ti and Zn–4Ti sample structures. Also, Fig. 8 shows images of cells in different extraction percentages for both samples. The control sample, Cell Culture Medium, does not extract from the metal sample. The alloys showed high toxicity effects in 100 and 50 percent extraction concentrations. However, the main difference between the two alloy structures is observed in 25 and 12 percent extraction concentrations. As we can see, the safe and suitable concentrations of ions released from Zn–4Ti alloy for MG-63 cells are in 25 and 12 percent extractions and showed a high survival effect on these cells. We can examine this survival difference from the related images in Fig. 8. The reason for this difference is naturally due to the difference in titanium percentage in the structures, which, by reducing titanium percentage from 10 percent to 4 percent, survival has significantly increased. Of course, both structures showed similar behavior in extractions with high purity. The main difference between the two structures is observed in 25 percent concentration, which significantly differs in cell survival. According to corrosion test results, Zn–10Ti alloy has weaker corrosion resistance behavior than Zn–4Ti alloy, and corrosion of this structure occurred faster. The effect of this process is evident in cell survival behavior because corrosion of alloy with higher speed leaves a negative effect on cell survival. Therefore, Zn–4Ti alloy showed much better survival behavior due to reduced corrosion speed. In previous studies on pure zinc metal survival, high toxicity has been reported due to the excessive release of zinc metal ions [53]. Considering the better performance of the Zn–4Ti structure, we can reach the standard ion release range with some precautions, such as surface coating, and use this alloy more for biodegradable implants.

4. Conclusion

In this study, the powder metallurgy method fabricated an alloy of zinc metal with 4 and 10 percent titanium (Zn–4Ti and Zn–10Ti) and characterized it as a material for biodegradable implants. XRD results indicate the formation of the intermetallic compound TiZn16 in both alloys and the TiZn3 compound in Zn–10Ti. Microscopic results show an almost uniform distribution of titanium in the zinc matrix while increasing the titanium percentage to 10 percent. Areas with titanium accumulation are observed. The porosity percentage in Zn–4Ti sample (1.85 %) is less than Zn–10Ti (4 %). The hardness of Zn–10Ti and Zn–4Ti (respectively 237 and 125 Vickers) are 4 to 2 times higher than pure zinc (60 Vickers). Corrosion results indicate more negative potential and lower current density of Zn–4Ti. In the impedance test, Zn–4Ti shows better corrosion resistance. To evaluate the cell toxicity of fabricated alloys, the survival of MG-63 cells was performed by an indirect method using an extraction process. The results showed that fabricated zinc alloy with a lower titanium percentage (Zn–4Ti) could be considered a candidate for biodegradable implants due to lower corrosion rate and better cell behavior.

CRediT authorship contribution statement

Seyed Amirhossein Salahi: Writing – original draft, Visualization, Validation, Methodology, Investigation, Data curation. **Nahid Hassanzadeh Nemati:** Writing – review & editing, Writing – original draft, Supervision, Project administration, Methodology, Conceptualization. **Sayed Khatiboleslam Sadrnezhaad:** Writing – review & editing, Writing – original draft, Visualization, Supervision, Methodology, Conceptualization. **Ghasem Najafpour Darzi:** Writing – review & editing, Supervision, Methodology, Conceptualization.

Declaration of competing interest

The authors declare that they have no known competing financial interests or personal relationships that could have appeared to influence the work reported in this paper.

Data availability

No data was used for the research described in the article.

Acknowledgements

This research did not receive any specific grant from funding agencies in the public, commercial, or not-for-profit sectors.

References

[1] J. Jeong, J.H. Kim, J.H. Shim, N.S. Hwang, C.Y. Heo, Bioactive calcium phosphate materials and applications in bone regeneration, Biomater. Res. 23 (1) (2019), https://doi.org/10.1186/s40824-018-0149-3.
[2] T. Kim, C.W. See, X. Li, D. Zhu, Orthopedic implants and devices for bone fractures and defects: past, present and perspective, Eng. Regen. 1 (2020), https://doi.org/10.1016/j.engreg.2020.05.003.
[3] Y. Yang, C. He, E. Dianyu, W. Yang, F. Qi, D. Xie, C. Shuai, Mg bone implant: features, developments and perspectives, Mater. Des. (2020), https://doi.org/10.1016/j.matdes.2019.108259.
[4] I. Cockerill, I. Cockerill, Y. Su, J.H. Lee, D. Berman, M.L. Young, Y. Zheng, D. Zhu, Micro-/Nanotopography on bioresorbable zinc dictates cytocompatibility, bone cell differentiation, and macrophage polarization, Nano Lett. 20 (6) (2020), https://doi.org/10.1021/acs.nanolett.0c01448.
[5] W. Wang, K.W.K. Yeung, Bone grafts and biomaterials substitutes for bone defect repair: a review, Bioact. Mater. 2 (Issue 4) (2017), https://doi.org/10.1016/j.bioactmat.2017.05.007.
[6] N. Haghani, N. Hassanzadeh Nemati, M.T. Khorasani, S. Bonakdar, Fabrication of polycaprolactone/heparinized nano fluorohydroxyapatite scaffold for bone tissue engineering uses, Int. J. Poly. Mater. Poly. Biomater. (2023), https://doi.org/10.1080/00914037.2023.2182781.
[7] H. Qu, H. Fu, Z. Han, Y. Sun, Biomaterials for bone tissue engineering scaffolds: a review, RSC Adv. 9 (Issue 45) (2019), https://doi.org/10.1039/c9ra05214c.
[8] E. Hosseinzadeh, M. Davarpanah, N. Hassanzadeh Nemati, S.A. Tavakoli, Fabrication of a hard tissue replacement using natural hydroxyapatite derived from bovine bones by thermal decomposition method, Int. J. Organ Transplant. Med. 5 (1) (2014) 23–31. https://pubmed.ncbi.nlm.nih.gov/25013675/.
[9] S.M. Mirhadi, N. Hassanzadeh Nemati, Synthesis and characterization of highly porous TiO2 scaffolds for bone defects, Int. J. Eng. Transact. A: Basics 33 (1) (2020), https://doi.org/10.5829/ije.2020.33.01a.15.
[10] J. Zhang, Y. Jiang, Z. Shang, B. Zhao, M. Jiao, W. Liu, M. Cheng, B. Zhai, Y. Guo, B. Liu, X. Shi, B. Ma, Biodegradable metals for bone defect repair: a systematic review and meta-analysis based on animal studies, Bioact. Mater. 6 (Issue 11) (2021), https://doi.org/10.1016/j.bioactmat.2021.03.035.
[11] R. Krishnan, S. Pandiaraj, S. Muthusamy, H. Panchal, M.S. Alsoufi, A.M. M. Ibrahim, A. Elsheikh, Biodegradable magnesium metal matrix composites for biomedical implants: synthesis, mechanical performance, and corrosion behavior - a review, J. Mater. Res. Technol. 20 (2022), https://doi.org/10.1016/j.jmrt.2022.06.178.
[12] F. Xing, S. Li, D. Yin, J. Xie, P.M. Rommens, Z. Xiang, M. Liu, U. Ritz, Recent progress in Mg-based alloys as a novel bioabsorbable biomaterials for orthopedic applications, J. Magnesium Alloys 10 (Issue 6) (2022), https://doi.org/10.1016/j.jma.2022.02.013.
[13] G.R. Dabbagh, S.K. Sadrnezhaad, R. Shoja Razavi, A.A. Nourbakhsh, N. Hassanzadeh Nemati, Laser textured novel patterns on Ti6Al4V alloy for dental implants surface improvement, J. Laser Appl. 33 (4) (2021), https://doi.org/10.2351/7.0000418.
[14] B. Rahnejat, N. Hassanzadeh Nemati, S.K. Sadrnezhaad, M.A. Shokrgozar, Promoting osteoblast proliferation and differentiation on functionalized and laser treated titanium substrate using hydroxyapatite/β-tricalcium phosphate/silver nanoparticles, Mater. Chem. Phys. 293 (2023), https://doi.org/10.1016/j.matchemphys.2022.126885.
[15] Y. Su, J. Fu, S. Du, E. Georgas, Y.X. Qin, Y. Zheng, Y. Wang, D. Zhu, Biodegradable Zn–Sr alloys with enhanced mechanical and biocompatibility for biomedical applications, Smart Mater. Med. 3 (2022), https://doi.org/10.1016/j.smaim.2021.12.004.
[16] X. Zhuo, Y. Wu, J. Ju, H. Liu, J. Jiang, Z. Hu, J. Bai, F. Xue, Recent progress of novel biodegradable zinc alloys: from the perspective of strengthening and toughening, J. Mater. Res. Technol. 17 (2022), https://doi.org/10.1016/j.jmrt.2022.01.004.
[17] H. Wu, X. Xie, J. Wang, G. Ke, H. Huang, Y. Liao, Q. Kong, Biological properties of Zn–0.04Mg–2Ag: a new degradable zinc alloy scaffold for repairing large-scale bone defects, J. Mater. Res. Technol. 13 (2021), https://doi.org/10.1016/j.jmrt.2021.05.096.
[18] X. Qu, H. Yang, B. Jia, Z. Yu, Y. Zheng, K. Dai, Biodegradable Zn–Cu alloys show antibacterial activity against MRSA bone infection by inhibiting pathogen adhesion and biofilm formation, Acta Biomater. 117 (2020), https://doi.org/10.1016/j.actbio.2020.09.041.
[19] M.W. Ghani Fahmi, A.F. Trinanda, R.Y. Pratiwi, S. Astutiningtyas, A. Zakiyuddin, The effect of Zr addition on microstructures and hardness properties of Zn-Zr alloys for biodegradable orthopaedic implant applications. IOP conference series: Mater. Sci. Eng. 833 (1) (2020) https://doi.org/10.1088/1757-899X/833/1/012065.

[20] S. Zhu, C. Wu, G. Li, Y. Zheng, J.F. Nie, Microstructure, mechanical properties and creep behaviour of extruded Zn-xLi (x = 0.1, 0.3 and 0.4) alloys for biodegradable vascular stent applications, Mater. Sci. Eng., A 777 (2020), https://doi.org/10.1016/j.msea.2020.139082.
[21] A.A. Oliver, R.J. Guillory, K.L. Flom, L.M. Morath, T.M. Kolesar, E. Mostaed, M. Sikora-Jasinska, J.W. Drelich, J. Goldman, Analysis of vascular inflammation against bioresorbable Zn-Ag-based alloys, ACS Appl. Bio Mater. 3 (10) (2020), https://doi.org/10.1021/acsabm.0c00740.
[22] P.K. Bowen, J.M. Seitz, R.J. Guillory, J.P. Braykovich, S. Zhao, J. Goldman, J. W. Drelich, Evaluation of wrought Zn–Al alloys (1, 3, and 5 wt % Al) through mechanical and in vivo testing for stent applications, J. Biomed. Mater. Res. B Appl. Biomater. 106 (1) (2018), https://doi.org/10.1002/jbm.b.33850.
[23] D. Nečas, I. Marek, J. Pinc, D. Vojtěch, J. Kubásek, Advanced zinc–magnesium alloys prepared by mechanical alloying and spark plasma sintering, Materials 15 (15) (2022), https://doi.org/10.3390/ma15155272.
[24] A. Kafri, S. Ovadia, G. Yosafovich-Doitch, E. Aghion, The effects of 4%Fe on the performance of pure zinc as biodegradable implant material, Ann. Biomed. Eng. (2019), https://doi.org/10.1007/s10439-019-02245-w.
[25] J.A. Carvalho, M.T. Fernandes, A.A. Ribeiro, J.A. Castro, In-Vitro evaluation of Zn-42Mg-4Ca alloy fabricated by powder metallurgy as a biodegradable biomaterial, Int. J. Develop. Res. 11 (February) (2021) 43935–43942, https://doi.org/10.37118/ijdr.20924.01.2021.
[26] J. Kubásek, D. Dvorský, J. Čapek, S. Marketa, H. Klara, D. Vojtěch, Zinc alloys as prospective materials for biodegradable medical devices, Manufact. Technol. 20 (6) (2020), https://doi.org/10.21062/MFT.2020.113.
[27] C. Gao, C. Li, S. Peng, C. Shuai, Spiral-eutectic-reinforced biodegradable Zn–Mg–Ag alloy prepared via selective laser melting, Chin. J. Mech. Eng.: Additive Manuf. Front. 1 (2) (2022), https://doi.org/10.1016/j.cjmeam.2022.100022.
[28] W. Zhang, P. Li, G. Shen, X. Mo, C. Zhou, D. Alexander, F. Rupp, J. Geis-Gerstorfer, H. Zhang, G. Wan, Appropriately adapted properties of hot-extruded Zn–0.5Cu–xFe alloys aimed for biodegradable guided bone regeneration membrane application, Bioact. Mater. 6 (4) (2021), https://doi.org/10.1016/j.bioactmat.2020.09.019.
[29] N. Gopal, P. Palaniyandi, P. Ramasamy, H. Panchal, A.M.M. Ibrahim, M.S. Alsoufi, A.H. Elsheikh, *In Vitro* Degradability,Microstructural evaluation, and biocompatibility of Zn-Ti-Cu-Ca-P alloy, Nanomaterials 12 (1357) (2022), https://doi.org/10.3390/nano12081357.
[30] S. Hagelstein, S. Zankovic, A. Kovacs, R. Barkhoff, M. Seidenstuecker, Mechanical analysis and corrosion analysis of zinc alloys for bioabsorbable implants for osteosynthesis, Materials 15 (2) (2022), https://doi.org/10.3390/ma15020421.
[31] M. Berger, E. Rubinraut, I. Barshack, A. Roth, G. Keren, J. George, Zinc reduces intimal hyperplasia in the rat carotid injury model, Atherosclerosis 175 (2) (2004) 229–234, https://doi.org/10.1016/j.atherosclerosis.2004.03.022.
[32] Z. Yin, Microstructural evolution and mechanical properties of Zn-Ti alloys for biodegradable stent applications, Maste. Sci. Mater. Sci. Eng. (2017), https://doi.org/10.37099/mtu.dc.etdr/553.
[33] K. Wang, X. Tong, J. Lin, A. Wei, Y. Li, M. Dargusch, C. Wen, Binary Zn–Ti alloys for orthopedic applications: corrosion and degradation behaviors, friction and wear performance, and cytotoxicity, J. Mater. Sci. Technol. 74 (2021), https://doi.org/10.1016/j.jmst.2020.10.031.
[34] G.T. Sudha, B. Stalin, M. Ravichandran, M. Balasubramanian, Mechanical properties, characterization and wear behavior of powder metallurgy composites-A review, Mater. Today: Proc. 22 (2019), https://doi.org/10.1016/j.matpr.2020.03.389.
[35] Y. Narendra Kumar, B. Venkateswarlu, L. Ratna Raju, R. Dumpala, B. Ratna Sunil, Developing Zn-MgO composites for degradable implant applications by powder metallurgy route, Mater. Lett. 302 (2021), https://doi.org/10.1016/j.matlet.2021.130433.
[36] P. Srikar, T. Sathish, P.I. Khan, Y.K. Reddy, V.V. Kondaiah, M.A. Rao, R. Dumpala, B.R. Sunil, Zinc-calcium silicate composites produced by ball milling and sintering for degradable implant applications, Mater. Today: Proc. 44 (2021), https://doi.org/10.1016/j.matpr.2020.11.785.
[37] G. SathishKumar, P. Parameswaran, V. Vijayan, R. Yokeswaran, Effects of Ca, Cu concentration on degradation behavior of Zn alloys in Hank's solution, Met. Powder Rep. 76 (1) (2021), https://doi.org/10.1016/j.mprp.2019.12.005.
[38] G. Arunkumar, A.M. Rameshbabu, P. Parameswaran, T.R. Kumar, K.R. Krishnan, Microstructural, cytotoxicity and antibacterial properties of bio-degradable Zn-2Cu-Ti alloy, Mater. Today: Proc. 37 (Part 2) (2020), https://doi.org/10.1016/j.matpr.2020.09.449.
[39] A. Owhal, A.D. Pingale, S.U. Belgamwar, J.S. Rathore, Preparation of novel Zn/Gr MMC using a modified electro-co-deposition method: microstructural and tribo-mechanical properties, Mater. Today: Proc. 44 (2021), https://doi.org/10.1016/j.matpr.2020.09.459.
[40] F. An, Z. Ma, K. Sun, L. Zhang, S.J. Na, J. Ning, H. Yu, Influences of the Ag content on microstructures and properties of Zn–3Mg–xAg alloy by spark plasma sintering, J. Mater. Res. Technol. 24 (2023) 595–607, https://doi.org/10.1016/j.jmrt.2023.03.051.
[41] M. Abedi, S. Sovizi, A. Azarniya, D. Giuntini, M.E. Seraji, H.R.M. Hosseini, An analytical review on Spark Plasma Sintering of metals and alloys: from processing window, phase transformation, and property perspective, Crit. Rev. Solid State Mater. Sci. 48 (2) (2022) 169–214, https://doi.org/10.1080/10408436.2022.2049441.
[42] J. Lin, X. Tong, K. Wang, Z. Shi, Y. Li, M. Dargusch, C. Wen, Biodegradable Zn–3Cu and Zn–3Cu–0.2Ti alloys with ultrahigh ductility and antibacterial ability for orthopedic applications, J. Mater. Sci. Technol. 68 (2021), https://doi.org/10.1016/j.jmst.2020.06.052.
[43] J. Lin, X. Tong, Z. Shi, D. Zhang, L. Zhang, K. Wang, A. Wei, L. Jin, J. Lin, Y. Li, C. Wen, A biodegradable Zn-1Cu-0.1Ti alloy with antibacterial properties for orthopedic applications, Acta Biomater. 106 (2020), https://doi.org/10.1016/j.actbio.2020.02.017.
[44] G.P. Vassilev, X.J. Liu, K. Ishida, Reaction kinetics and phase diagram studies in the Ti-Zn system, J. Alloys Compd. 375 (1–2) (2004), https://doi.org/10.1016/j.jallcom.2003.11.026.
[45] H. Okamoto, Ti-Zn (Titanium-Zinc), J. Phase Equilibria Diffus. 29 (2) (2008), https://doi.org/10.1007/s11669-008-9271-6.
[46] L. Zhang, X.Y. Liu, H. Huang, W. Zhan, Effects of Ti on microstructure, mechanical properties and biodegradation behavior of Zn-Cu alloy, Mater. Lett. 244 (2019), https://doi.org/10.1016/j.matlet.2019.02.071.
[47] O.M. Suárez, E.G. Estremera, R. Soler, A. Declet, A.J. Hernández-Maldonado, Fabrication of porous and nanoporous aluminum via selective dissolution of Al-Zn alloys, Adv. Mater. Sci. Eng. (2014), https://doi.org/10.1155/2014/963042.
[48] F. Sánchez, A. Bolarm, P. Molera, Relationship between particle size and manufacturing processing and sintered characteristics of iron powders, de Metalurgia y 23 (2003). https://api.semanticscholar.org/CorpusID:137136018.
[49] G. Manohar, K.M. Pandey, S.R. Maity, Effect of sintering mechanisms on mechanical properties of AA7075/B4C composite fabricated by powder metallurgy techniques, Ceram. Int. 47 (11) (2021), https://doi.org/10.1016/j.ceramint.2021.02.073.
[50] G. Ghosh, S. Delsante, G. Borzone, M. Asta, R. Ferro, Phase stability and cohesive properties of Ti-Zn intermetallics: first-principles calculations and experimental results, Acta Mater. 54 (19) (2006), https://doi.org/10.1016/j.actamat.2006.04.038.
[51] J.G. Miranda-Hernández, H. Herrera-Hernández, C.O. González-Morán, J.N. Rivera Olvera, I. Estrada-Guel, F. Botello Villa, Synthesis and characterization of Zn-nix advanced alloys prepared by mechanical milling and sintering at solid-state process, Adv. Mater. Sci. Eng. (2017), https://doi.org/10.1155/2017/7967848.
[52] M.S. Ardakani, Engineering Mechanically-Stable Zinc-Based Alloys for Medical Implants, [Michigan Technological University], 2022, https://doi.org/10.37099/mtu.dc.etdr/1409.
[53] M. Wątroba, W. Bednarczyk, P.K. Szewczyk, J. Kawałko, K. Mech, A. Grünewald, I. Unalan, N. Taccardi, G. Boelter, M. Banzhaf, C. Hain, P. Bała, A.R. Boccaccini, In vitro cytocompatibility and antibacterial studies on biodegradable Zn alloys supplemented by a critical assessment of direct contact cytotoxicity assay, J. Biomed. Mater. Res. B Appl. Biomater. 111 (2) (2023), https://doi.org/10.1002/jbm.b.35147.